# Equivalent Series Resistance-based Real-time Control for a Battery-Ultracapacitor Hybrid System

Chen Zhao, He Yin
Univ. of Michigan-Shanghai Jiao Tong Univ. Joint Institute,
Shanghai Jiao Tong University,
Shanghai, P. R. China
Email: chenzhaosjtu@gmail.com
yyy@sjtu.edu.cn

Zhongping Yang
School of Electrical Engineering
Beijing Jiao Tong University,
Beijing, P. R. China
Email: zhpyang@bjtu.edu.cn

Chengbin Ma*[1,2]
1. Univ. of Michigan-Shanghai Jiao Tong Univ. Joint Institute,
2. School of Mechanical Engineering,
Shanghai Jiao Tong University,
Shanghai, P. R. China
Email: chbma@sjtu.edu.cn

***Abstract*—This paper provides an equivalent series resistance-based real-time control method for the battery-ultracapacitor hybrid system. The idea of this control method is that the dynamic load demand is distributed based on the equivalent series resistance ratio of batteries to ultracapacitors, whilst the estimated average load demand based on the past $N$ seconds is supplied by the batteries. In addition, the energy stored in the ultracapacitors is considered for protection purpose. The simulation results verify the effectiveness of the equivalent series resistance-based real-time control method, in terms of the system efficiency, the overall energy loss, and the utilization of the ultracapacitors. Further comparison results show that the efficiency of the proposed real-time control method with well-selected parameter is only 1% lower than that of the dynamic programming method.**

***Index Terms*—Hybrid energy system, Equivalent series resistance, Real-time control, Battery, Ultracapacitor**

## I. Introduction

The traditional internal combustion engines (ICEs) act as the energy source in industries (e.g., automotives, ships, locomotives, etc.) since 19th century. In order to reduce the $CO_2$ emission and improve the fuel economy of the ICEs, many energy generators (Fuel cell, PV panel, wind turbine, etc.) and energy storage devices (battery, ultracapacitor (UC), flywheel, etc.) are proposed [1], [2]. In order to meet the load demand with high efficiency and reliability, a hybrid energy system (HES) with multiple energy generators and energy storage devices is proved to be a feasible solution [3]. Due to the different characteristics of the energy devices, optimal energy management of the hybrid energy system is a challenging task [4].

In the HESs, the energy flow between the different energy devices needs to be controlled to improve the system efficiency, reliability, and robustness. Therefore, many energy management strategies have been proposed and can be classified into two groups: rule-based and optimization-based methods [5], [6]. Many rule-based methods have been proposed, due to its simplicity and flexibility in real-time implementation [7]–[11]. The hysteresis control method was proposed to keep the energy stored in the high-efficient energy buffer within its favourable range [7]. The low-pass filter and wavelet-transform were used to distribute load power to each energy devices according to their response time [8], [9]. Fuzzy logic was shown to be suitable for the control of the HES [10], [11]. However, the performance of the optimization-based methods is always better than that of the rule-based methods because it directly minimizes the cost function defined by users [6]. An optimal-control-model method was discussed to minmize the fuel consumption [12]. Model predictive control was able to handle various constraints in the HES [13]. The offline dynamic programming (DP) method was utilized to minimize the energy loss, fuel consumption, and costs of the HES [14]–[16]. However, these optimization-based methods are only valid with a prior knowledge of driving cycle and cannot be implemented in real-time. The near-optimal real-time control methods were proposed by using the optimization results to train the neural networks or redesign the parameters of the rule-based method [12], [14], [16]. But it needs the optimization results under all the possible load profiles, which is not cost-effective.

Apart from focusing on the optimization results searched by optimization-based methods, the models of the HES can provide a hint for load distribution between different energy devices. It is found that the loss ratio between different energy devices determines which energy device is more efficient under a same load demand [17]. From the energy loss minimization point of view, it is theorectically proved that the optimal load distribution is determined by the equivalent series resistance (ESR) ratio between different energy devices [18]. Therefore, an ESR-based real-time control method is proposed, in which the battery-UC hybrid system is chosen as an example of the HES. In the proposed control method, the estimated average load power is supplied by the high energy density batteries, and the remaining dynamic load power is distributed based on the ESR-ratio of batteries to UCs and the SOC of the UCs. The simulation results show that an accurate algorithm to estimate average load power and the UC energy correction factor are needed to reduce the overall energy loss. Detailed comparison results show that the ESR-based real-time control method is comparable to the offline DP method.

## II. System configuration and modeling

### A. Topology

The different types of the battery-UC hybrid system are reviewed in [19]. With a single DC-DC converter, two semiactive topologies are possible, i.e., capacitor semiactive and battery semiactive hybrids. In the battery semiactive hybrid topology, the DC-DC converter is placed between the battery and the load. The battery semiactive hybrid is capable of controlling the battery working at near-average power, therefore reducing the power rating of the DC-DC converter [4], [7], [20]. But a large-sized UC is needed to maintain the DC bus voltage within its allowable range. In the capacitor semiactive hybrid topology, a DC-DC converter is connected between the UC and the load so that the energy stored in the UC can be fully utilized. But a high-power DC-DC converter is needed to charge and discharge the UC [12], [15], [16], [21]. In this work, the capacitor semiactive topology is chosen as an example to demonstrate the ESR-based real-time control method.

### B. Model of Battery-UC Hybrid System

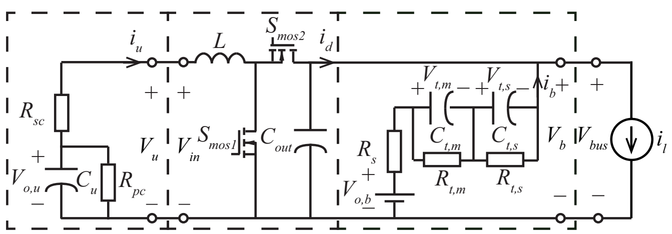


Fig. 1. Dynamic model for the capacitor semiactive hybrid system used in simulation.

*1) Battery model:* In this system-level analysis, the equivalent circuit model is used for the lithium-ion battery pack (4S2P), as shown in Fig. 1. $V_{o,b}$ is the open circuit voltage (OCV) of the battery and $R_s$ is the battery internal resistance. The two RC networks with different time constants, $\tau_s = R_{t,s}C_{t,s}$ and $\tau_m = R_{t,m}C_{t,m}$, model the transient voltage responses of the battery in second and minute ranges, respectively [22]. The model parameters listed in Table I are obtained using fast averaging method [23]. $V_{o,b}$ and $R_s$ are represented by the sixth-order polynomials

$$V_{o,b} = a_0 + a_1 x + a_2 x^2 + ... + a_6 x^6, \quad (1)$$
$$R_s = b_0 + b_1 x + b_2 x^2 + ... + b_6 x^6, \quad (2)$$

where $x$ is a specific $\text{SOC}_b$ [24]. The parameters of the two RC networks, $R_{t,s}$, $C_{t,s}$, $R_{t,m}$, $C_{t,m}$ are assumed to be constant. The power loss of the battery pack $P_{loss,b}$ can be written as

$$P_{loss,b} = R_s i_b^2 + \frac{V_{t,m}^2}{R_{t,m}} + \frac{V_{t,s}^2}{R_{t,s}} \quad (3)$$

where $i_b$ is the battery current.

*2) UC Model:* Again for the system-level analysis, the first-order electrical model is sufficient to represent the behavior of the UC pack (6S1P) [25] [see Fig. 1]. $V_{o,u}$ is the OCV of the UC pack. $R_{sc}$ is its internal resistance and $R_{pc}$ models the leak current [26]. The model parameters are listed in Table I. The power loss of the UC pack $P_{loss,u}$ can be represented as

$$P_{loss,u} = R_{sc} i_u^2 + \frac{V_{o,u}^2}{R_{pc}}, \quad (4)$$

where $i_u$ is the UC current.

*3) DC-DC converter loss model:* A half-bridge bidirectional DC-DC converter is used in the capacitor semiactive hybrid system [see Fig. 1], because it is more efficient than the Luk and SEPIC/Luo converter [1], [27]. Its power loss $P_{loss,d}$ can be approximately calculated using the first-order model of DC-DC converter [28]. In the model, switching duty cycle $d_s$ and average inductor current $i_L$ are used to estimate the losses in MOSFET switch $S_{mos1}$, $S_{mos2}$, and inductor $L$. Because the gate drive power loss of the DC-DC converter is usually small, the power loss can be expressed as

$$P_{loss,d} = V_{in} f_s Q_{mos} + (R_{mos} + R_L) i_L^2 \approx (R_{mos} + R_L) i_L^2, \quad (5)$$

where $V_{in}$ is the input voltage of the DC-DC converter; $f_s$ is the switching frequency of the DC-DC converter; $Q_{mos}$ is the gate charge of the MOSFET switch $S_{mos1}$ and $S_{mos2}$; $R_{mos}$ is the on-resistance of $S_{mos1}$ and $S_{mos2}$; $R_L$ is the resistance of the inductor $L$. The parameter values of the DC-DC converter are also listed in Table I.

## III. Equivalent series resistance-based real-time control

The idea of the ESR-based real-time control is that the dynamic load demand is distributed based on the ESR ratio between different energy devices, whilst the average load demand is supplied by the high energy density device. In the battery-UC hybrid system, the average load demand is supplied by the batteries. Without a prior knowledge of the load profile, the average load power needs to be estimated. In addition, the SOC of the UC pack is also considered to prevent its overcharge and overdischarge. The detailed explaination of the ESR-based real-time control is shown below.

### A. Estimated Average Load Power

For any arbitrary power load, its load profile can be decomposed into a average load power and a dynamic load power. The average load power is supplied by the batteries due to its high energy density. Without a prior knowledge of load profile, the average load power needs to be estimated based on the historical data. In this paper, a simple moving average filter is adopted, in which the average load power during the past $N$ sampled load power $P_{l,a,k}^N$ is used to estimate the average load power over the load profile. Therefore, the estimated average load power $P_{l,a,k}^N$ and dynamic load power $P_{l,d,k}$ at time instant $k$ are given by

TABLE I
PARAMETERS FOR THE CAPACITOR SEMIACTIVE HYBRID SYSTEM.

| | | | | | | | | | | | |
|---|---|---|---|---|---|---|---|---|---|---|---|
| Battery Pack (4S2P) | | | | | | | | | | | |
| $a_0$ | 12.38 | $a_1$ | 29.02 | $a_2$ | -129.51 | $a_3$ | 299.09 | $a_4$ | -366.81 | $a_5$ | 231.77 |
| $a_6$ | -59.23 | $b_0$ | 0.49 | $b_1$ | -4.72 | $b_2$ | 28.51 | $b_3$ | -83.27 | $b_4$ | 125.62 |
| $b_5$ | -94.10 | $b_6$ | 27.67 | $R_{t,s}$ | 40 mΩ | $C_{t,s}$ | 400 F | $R_{t,m}$ | 8 mΩ | $C_{t,m}$ | 3000 F |
| UC Pack (6S1P) | | | | | | | | | | | |
| $C_u$ | 66 F | $R_{sc}$ | 15 mΩ | $R_{pc}$ | 10 kΩ | | | | | | |
| DC-DC Converter | | | | | | | | | | | |
| $R_{mos}$ | 15 mΩ | L | 200 uH | $R_L$ | 10 mΩ | $Q_{mos}$ | 75 nC | $f_s$ | 20 kHz | $C_{out}$ | 2000 uF |

$$P_{l,a,k}^N = \begin{cases} \frac{1}{k}\left(P_{l,a,k-1}^N \cdot (k-1) + P_{l,k}\right) & \text{if } k \le N, \\ \frac{1}{N}\left(P_{l,a,k-1}^N \cdot N + P_{l,k} - P_{l,k-N}\right) & \text{else,} \end{cases} \tag{6}$$
$$P_{l,d,k} = P_{l,k} - P_{l,a,k}^N,$$

where $P_{l,k}$ $P_{l,k-N}$ are the load power at time instant $k$ and $k-N$, respectively. $P_{l,a,k-1}^N$ is the estimated average load power at time instant $k-1$. Fig. 2 shows that the estimated average load power $P_{l,a,k}^N$ is close to the average load power $P_{l,a}$ as $N$ increases.

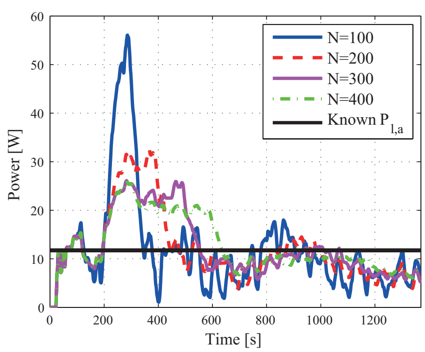


Fig. 2. Estimated average load power under different $N$.

## B. Load Distribution Based on the ESR Ratio

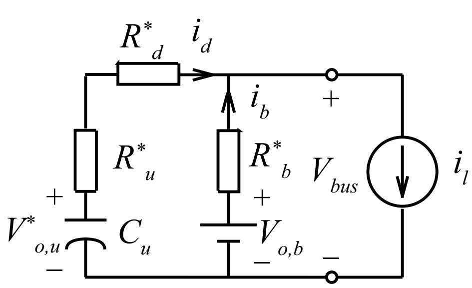

Fig. 3. ESR circuit for the capacitor semiactive hybrid system.

Fig. 3 shows the ESR circuit model of the battery-UC hybrid system, in which the capacitor semiactive topology is used. Because $R_s$ is usually much larger than $R_{t,s}$ and $R_{t,m}$, the power loss caused by $R_{t,s}$ and $R_{t,m}$ are neglected. Similarly, the power loss caused by leak-current resistance $R_{pc}$ in the UC model is neglected due to its large value. Therefore, the parameters of the ESR circuit are given by

$$R_b^* = \frac{P_{loss,b}}{i_d^2} \approx R_s, \quad R_d^* = \frac{P_{loss,d}}{i_d^2} \approx \frac{R_L + R_{mos}}{(1-d_s)^2},$$
$$R_u^* = \frac{P_{loss,u}}{i_u^2} \approx \frac{R_{sc}}{(1-d_s)^2}, \quad K = \frac{R_b^*}{R_d^* + R_u^*},$$

where the $d_s$ is the duty cycle of the DC-DC converter. It has been theoretically proved that in order to minimize the energy loss of the hybrid system, the optimal current distribution between the battery and UC packs is irrelevant to the load profile, but solely determined by the ESR ratio $K$ under a constant DC bus voltage [18]. A big ESR leads to a large power loss when supplying a same load. In the capacitor semiactive topology, the variation of the DC bus voltage is limited due to the flat voltage profile of the battery pack. Therefore, without considering the physical limits, $\frac{1}{K+1}$ of dynamic load current is supplied by the battery pack and the remaining dynamic part of the load current is supplied by the UC pack to minimize the overall energy loss [18]. In the proposed ESR-based control, $R_s$ is calculated using $\text{SOC}_{b,k}$ and $d_s$ is estimated as $1 - \frac{i_{d,k-1}}{i_{u,k-1}}$. Thus the ESR ratio $K$ is determined.

## C. Constraints of SOC Range of the UC pack

In the battery-UC hybrid system, the UC pack acts as the energy buffer to supply the dynamic part of the load power due to its high efficiency. However, due to the limited energy density, the SOC of the UC pack $\text{SOC}_u$ needs to be considered to prevent overcharge and overdischarge. Due to the equal chance of charging and discharging in the dynamic load power with zero average, $\text{SOC}_u$ is controlled to swing around 50% by introducing a linear energy correction factor $Q$, as shown below.

$$Q = \begin{cases} (2\text{SOC}_u - 1)\, K^{\frac{1+s}{2}} + 1 & \text{if } P_{l,d,k} \le 0, \\ (1 - 2\text{SOC}_u)\, K^{\frac{1-s}{2}} + 1 & \text{else,} \end{cases} \tag{7}$$
$$s = \text{sign}(\text{SOC}_u - 0.5), \quad \text{SOC}_u = \frac{V_{u,k}^2 - V_{u,min}^2}{V_{u,max}^2 - V_{u,min}^2},$$

where $V_{u,max}$ and $V_{u,min}$ are the maximum and minimum voltage of the UC pack. Then the currents of the battery pack and the DC-DC converter are written as

$$i_{b,k} = \frac{P_{l,a,k}^N}{V_{bus}} + C_d \frac{P_{l,k} - P_{l,a,k}^N}{V_{bus}}, \tag{8}$$

$$i_{d,k} = \frac{P_{l,k}}{V_{bus}} - i_{b,k}, \tag{9}$$

$$C_d = Q \frac{1}{1+K}, \tag{10}$$

$$V_{bus} = V_{o,b} - V_{t,s} - V_{t,m} - i_{b,k} R_s, \tag{11}$$

where $C_d$ denotes the percentage of dynamic load current that is supplied by the battery pack. Fig. 4 shows the relationship between current distribution $C_d$ and the SOC of the UC pack $\text{SOC}_u$ when the resistance ratio $K$ is 2. It shows that with a 50% $\text{SOC}_u$, the current distribution $C_d$ is set as the optimal value (i.e., $\frac{1}{1+K}$) to minimize the energy loss. When $\text{SOC}_u$ is higher than 50%, $C_d$ becomes smaller (larger) than the optimal $\frac{1}{1+K}$ under a positive (negative) $P_{l,d,k}$. Thus, the SOC of the UC pack $\text{SOC}_u$ decreases towards 50% by forcing the UC pack to supply more discharging power (capture less regenerative power). Under the extreme case with a 100% $\text{SOC}_u$, the UC pack supplies all the discharging power and the battery pack captures the entire regenerative power to avoid the overcharge of the UC pack. Similarly, when $\text{SOC}_u$ is lower than 50%, the UC pack tends to supply less discharging power and capature more regenerative power.

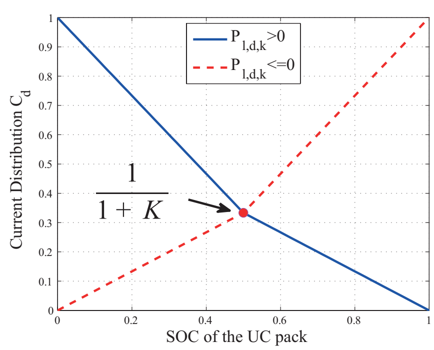


Fig. 4. Current distribution $C_d$ as a function of SOC of the UC pack $\text{SOC}_u$.

By combining (8)–(11), the current of the battery pack $i_{b,k}$ can be further written as

$$i_{b,k} = \frac{V_b' - \sqrt{V_b'^2 - 4R_s \left[\frac{Q}{1+K}(P_{l,k} - P_{l,a,k}^N) + P_{l,a,k}^N\right]}}{2R_s},$$

$$V_b' = V_{o,b} - V_{t,s} - V_{t,m}.$$

Fig. 5 shows the flow chart of the ESR-based real-time control. The reference battery current $i_{b,k}$ is calculated based on the $\text{SOC}_{b,k}$, $V_{u,k}$, $P_{l,k}$ at the time instant $k$ and $i_{d,k-1}$, $i_{u,k-1}$, $P_{l,a,k-1}^N$ at time instant $k-1$.

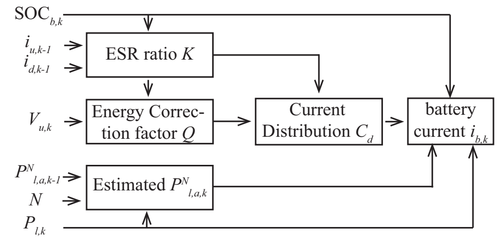


Fig. 5. Flow chart for the ESR-based real-time control method.

## IV. Simulation Result

Fig. 6 shows the downscaled power profiles of the urban dynamometer driving schedule (UDDS). The downscaled power profile of UDDS driving cycle is used here as an example of realistic power load profile. In simulation, the initial $\text{SOC}_b$ and $\text{SOC}_u$ are set to be 80% and 50%, respectively. Usually, the voltage range of the UC pack is between 50% and 100% of its maximum voltage $V_{u,max}$. Therefore, $V_{u,min}$ is set to be one half of $V_{u,max}$. The overall energy loss $E_{loss}$, the utilization of the UC pack $\Delta\text{SOC}_u$, and the system efficiency $\eta_s$ are used to evaluate the control performance. $\Delta\text{SOC}_u$ denotes the percentage of energy stored in the UC pack that is utilized over the load profile. A large $\Delta\text{SOC}_u$ indicates a high utilization of UC pack. The overall energy loss $E_{loss}$, the utilization of the UC pack $\Delta\text{SOC}_u$, and system efficiency $\eta_s$ are defined as

$$E_{loss} = \sum_{k=1}^{N} (P_{loss,b,k} + P_{loss,d,k} + P_{loss,u,k}) T_s,$$

$$\Delta\text{SOC}_u = \max_{1\le k\le N} \text{SOC}_{u,k} - \min_{1\le k\le N} \text{SOC}_{u,k},$$

$$\eta_s = \frac{E_{load}}{E_{dis}}, \quad E_{dis} = \sum_{k=1}^{N} (i_{b,k} V_{o,b} + i_{u,k} V_{o,u}) T_s,$$

where $T_s$ is the sampling time and $N$ is total number of the sampling points.

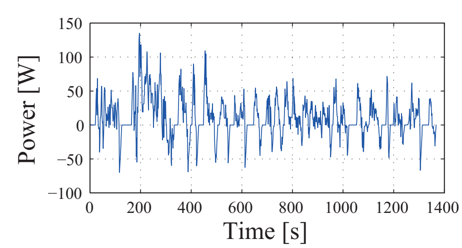


Fig. 6. Downscaled power profile of the UDDS driving cycle.

### A. Influence of Window Size $N$

Table II shows the simulation results of the ESR-based control under different window size $N$. It indicates that the system efficiency $\eta_s$ increases and the overall energy loss $E_{loss}$ decreases when $N$ increases. It is because more energy stored in the UC pack is utilized (i.e., a large $\Delta\text{SOC}_u$) as the estimated average load power is close to the average load power $P_{l,a}$, as shown in Fig. 2. It indicates that an accurate

TABLE II
SIMULATION RESULTS OF THE ESR-BASED REAL-TIME CONTROL UNDER DIFFERENT $N$ AND ONE SCALED UDDS POWER PROFILE.

| N | 100 | 200 | 300 | 400 |
|---|---|---|---|---|
| $E_{loss}$ | 645.7 | 596.0 | 588.4 | 586.2 |
| $\Delta \mathrm{SOC}_u$ | 0.389 | 0.446 | 0.476 | 0.527 |
| $\eta_s[\%]$ | 96.33 | 96.61 | 96.65 | 96.66 |

estimated average load power would lead to a high utilization of the UC pack and an efficient battery-UC hybrid system. Therefore, the window size of the moving average filter needs to be optimized to minimize the energy loss of the battery-UC hybrid system. It is noted that the optimal window size N depends on the specific load profile.

### *B. Influence of UC Energy Correction Factor $Q$*

TABLE III
SIMULATION RESULTS OF THE ESR-BASED REAL-TIME CONTROL METHOD UNDER DIFFERENT $N$ WHEN $Q = 1$.

| N | 100 | 200 | 300 | 400 |
|---|---|---|---|---|
| $E_{loss}$[J] | 601.6 | 556.1 | 553.1 | 556.6 |
| $\Delta \mathrm{SOC}_u$ | 0.361 | 0.457 | 0.520 | 0.596 |
| $\eta_s[\%]$ | 96.61 | 96.88 | 96.90 | 96.88 |

Table III shows that simulation results of the ESR-based real-time control method without the UC energy correction factor $Q$ (i.e., $Q$=1). Compared with the results in Table II, the battery-UC hybrid system is more efficient with a larger $\Delta \mathrm{SOC}_u$ and a lower $E_{loss}$ when $Q$=1. However, the largest $\Delta \mathrm{SOC}_u$ (0.596) does not lead to the highest efficiency due to the nonlinearilty of the battery-UC hybrid system. Therefore, it indicates that the $\Delta \mathrm{SOC}_u$ needs to be limited to avoid the efficiency drop caused by the deep charging and discharging of the UC pack.

### *C. Comparison with Dynamic Programming Method*

In order to verify the performance of the ESR-based real-time control method, its simulation results with the well-selected parameter is compared with the global optimal solution searched by the DP method, as shown in Fig. 7. Figs. 7(a)–(c) show that with a low $\mathrm{SOC}_u$, the proposed real-time control method extracts more energy from the battery pack to meet the peak load demand during 200–300s, compared with the DP method. After the peak load demand, the UC pack is charged to reach a 50% $\mathrm{SOC}_u$ rapidly during 300–400s. Similarly, with a high $\mathrm{SOC}_u$ the UC pack tends to supply more discharging power and capture less regenerative power during 400–800s. Fig. 7(d) shows that the non-optimal load distribution due to the low $\mathrm{SOC}_u$ during 200–400s leads to most of the additional energy loss using the ESR-based real-time control method, compared with the DP method. It indicates that a low $\mathrm{SOC}_u$ over the load period may degrade the efficiency of the battery-UC hybrid system.

Table IV shows that the battery-UC hybrid system is more efficient than the battery-only system, with at least 50% energy

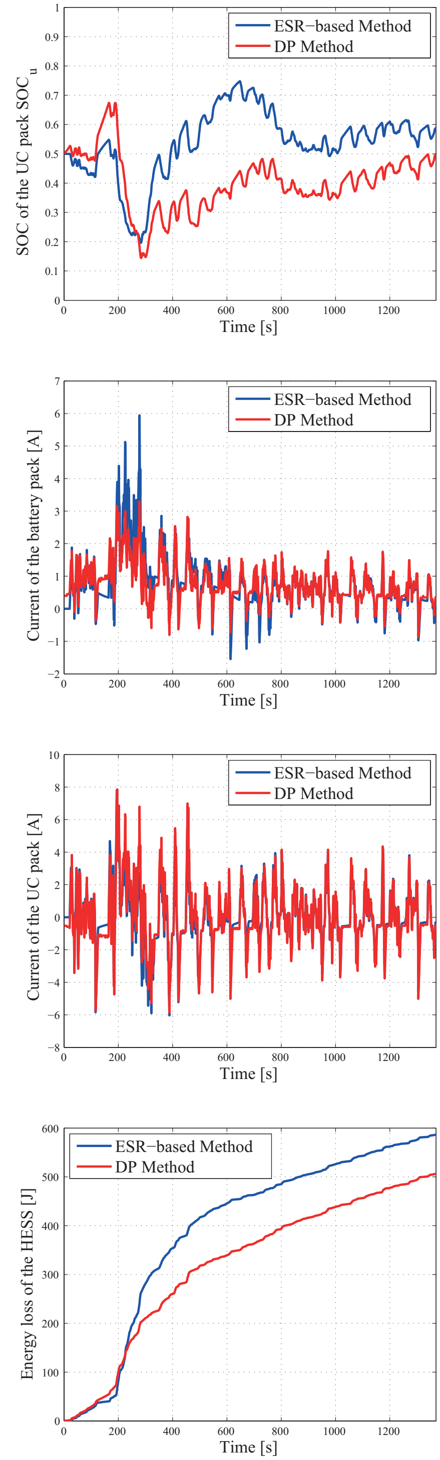


Fig. 7. Simulation results of the ESR-based real-time control method and the dynamic programming method. (a) SOC of the UC pack. (b) Current of the battery pack. (c) Current of the UC pack. (d) Overall energy loss.

TABLE IV
RESULTS OF DYNAMIC PROGRAMMING, ESR-BASED REAL-TIME METHOD (N=400), AND THE BATTERY-ONLY SYSTEM.

| Configuration | Battery-only | Battery-UC hybrid | |
|---|---|---|---|
| Method | N/A | Dynamic Programming | ESR-based (N=400) |
| $E_{loss}$[J] | 1302.1 | 506.1 | 586.2 |
| $\Delta\mathrm{SOC}_u$ | N/A | 0.530 | 0.527 |
| $\eta$[%] | 92.52 | 97.54 | 96.66 |

loss reduction. The utilization of the UC pack using the ESR-based control method and DP method are similar. The system efficiency using the ESR-ratio based real-time control method (N=400) is only 1% lower than that using the DP method. It indicates the ESR-based real-time control method is comparable to the DP method. This real-time method uses exponentiation and elementary arithmetic operations and does not require high computation power for implementation. In future, experiment results will validate its real-time capability.

## V. CONCLUSION

This paper provides an ESR-based real-time control method for the battery-UC hybrid system. The idea of the proposed control method is to distribute the dynamic load power based on the ESR ratio of battery pack to UC pack and SOC of the UC pack, and the estimated average load power is supplied by the batteries. The average load power during the past $N$ seconds is used to estimate the average load power over the load profile. The simulation results show that the system efficiency increases with an increased accuracy of average load power estimation. The deep charging and discharging of the UC pack should be avoided to realize an efficient battery-UC hybrid system. Detailed comparison results show that the proposed real-time control method can achieve a near-optimal performance, with only efficiency drop of 1% compared with the DP method. This efficiency drop is mainly caused by extracting more energy from the batteries due to a low $\mathrm{SOC}_u$. The further work includes the optimal design of an UC energy correction factor $Q$ and an accurate algorithm to estimate the average load power.

## REFERENCES


[1] S. F. Tie and C. W. Tan, "A review of energy sources and energy management system in electric vehicles," *Renew. Sust. Energ. Rev.*, vol. 20, pp. 82–102, 2013.

[2] S. M. Lukic, J. Cao, R. C. Bansal, F. Rodríguez, and A. Emadi, "Energy storage systems for automotive applications," *IEEE Trans. Ind. Electron.*, vol. 55, no. 6, pp. 2258–2267, 2008.

[3] P. Thounthong, S. Rael, and B. Davat, "Energy management of fuel cell/battery/supercapacitor hybrid power source for vehicle applications," *J. Power Sources*, vol. 193, no. 1, pp. 376–385, 2009.

[4] H. Yin, C. Zhao, M. Li, and C. Ma, "Utility function-based real-time control of a battery-ultracapacitor hybrid energy system," *IEEE Trans. Ind. Inf.*, vol. 11, no. 1, pp. 220–231, 2015.

[5] F. R. Salmasi, "Control strategies for hybrid electric vehicles: Evolution, classification, comparison, and future trends," *IEEE Trans. Veh. Technol.*, vol. 56, no. 5, pp. 2393–2404, 2007.

[6] S. G. Wirasingha and A. Emadi, "Classification and review of control strategies for plug-in hybrid electric vehicles," *IEEE Trans. Veh. Technol.*, vol. 60, no. 1, pp. 111–122, 2011.

[7] J. Cao and A. Emadi, "A new battery/ultracapacitor hybrid energy storage system for electric, hybrid, and plug-in hybrid electric vehicles," *IEEE Trans. Power Electron.*, vol. 27, pp. 122–132, Jan. 2012.

[8] E. Schaltz, A. Khaligh, and P. O. Rasmussen, "Influence of battery/ultracapacitor energy-storage sizing on battery lifetime in a fuel cell hybrid electric vehicle," *IEEE Trans. Veh. Technol.*, vol. 58, no. 8, pp. 3882–3891, 2009.

[9] X. Zhang, C. C. Mi, A. Masrur, and D. Daniszewski, "Wavelet-transform-based power management of hybrid vehicles with multiple on-board energy sources including fuel cell, battery and ultracapacitor," *J. Power Sources*, vol. 185, no. 2, pp. 1533–1543, 2008.

[10] M. Zandi, A. Payman, J.-P. Martin, S. Pierfederici, B. Davat, and F. Meibody-Tabar, "Energy management of a fuel cell/supercapacitor/battery power source for electric vehicular applications," *IEEE Trans. Veh. Technol.*, vol. 60, pp. 433–443, Feb. 2011.

[11] D. Rotenberg, A. Vahidi, and I. Kolmanovsky, "Ultracapacitor assisted powertrains: Modeling, control, sizing, and the impact on fuel economy," *IEEE Trans. Control Syst. Technol.*, vol. 19, pp. 576–589, May 2011.

[12] J. Moreno, M. E. Ortúzar, and J. W. Dixon, "Energy-management system for a hybrid electric vehicle, using ultracapacitors and neural networks," *IEEE Trans. Ind. Electron.*, vol. 53, pp. 614–623, Apr. 2006.

[13] A. Vahidi, A. Stefanopoulou, and H. Peng, "Current management in a hybrid fuel cell power system: A model-predictive control approach," *IEEE Trans. Control Syst. Technol.*, vol. 14, no. 6, pp. 1047–1057, 2006.

[14] C.-C. Lin, H. Peng, J. W. Grizzle, and J.-M. Kang, "Power management strategy for a parallel hybrid electric truck," *IEEE Trans. Control Syst. Technol.*, vol. 11, no. 6, pp. 839–849, 2003.

[15] A. Santucci, A. Sorniotti, and C. Lekakou, "Power split strategies for hybrid energy storage systems for vehicular applications," *J. Power Sources*, vol. 258, pp. 395–407, 2014.

[16] Z. Song, H. Hofmann, J. Li, X. Han, and M. Ouyang, "Optimization for a hybrid energy storage system in electric vehicles using dynamic programing approach," *Appl. Energy*, vol. 139, pp. 151–162, 2015.

[17] O. Laldin, M. Moshirvaziri, and O. Trescases, "Predictive algorithm for optimizing power flow in hybrid ultracapacitor/battery storage systems for light electric vehicles," *IEEE Trans. Power Electron.*, vol. 28, pp. 3882–3895, Aug. 2013.

[18] C. Zhao, H. Yin, Z. Yang, and C. Ma, "Equivalent series resistance-based energy loss analysis of a battery semiactive hybrid energy storage system," *IEEE Trans. Energy Convers.*, 2015, doi: "10.1109/TEC.2015.2418818".

[19] I. Aharon and A. Kuperman, "Topological overview of powertrains for battery-powered vehicles with range extenders," *IEEE Trans. Power Electron.*, vol. 26, no. 3, pp. 868–876, 2011.

[20] A. Kuperman, I. Aharon, S. Malki, and A. Kara, "Design of a semi-active battery-ultracapacitor hybrid energy source," *IEEE Trans. Power Electron.*, vol. 28, pp. 806–815, Feb. 2013.

[21] M. Ortúzar, J. Moreno, and J. Dixon, "Ultracapacitor-based auxiliary energy system for an electric vehicle: Implementation and evaluation," *IEEE Trans. Ind. Electron.*, vol. 54, no. 4, pp. 2147–2156, 2007.

[22] M. Chen and G. A. Rincon-Mora, "Accurate electrical battery model capable of predicting runtime and IV performance," *IEEE Trans. Energy Convers.*, vol. 21, no. 2, pp. 504–511, Jun. 2006.

[23] S. Abu-Sharkh and D. Doerffel, "Rapid test and non-linear model characterisation of solid-state lithium-ion batteries," *J. Power Sources*, vol. 130, pp. 266–274, May 2004.

[24] R. C. Kroeze and P. T. Krein, "Electrical battery model for use in dynamic electric vehicle simulations," in *Proc. IEEE Power Electronics Specialists (PESC'2008)*, Rhodes, Greece, Jun. 2008, pp. 1336–1342.

[25] M. Mellincovsky, A. Kuperman, C. Lerman, S. Gadelovits, I. Aharon, N. Reichbach, G. Geula, and R. Nakash, "Performance and limitations of a constant power-fed supercapacitor," *IEEE Trans. Energy Convers.*, vol. 29, no. 2, pp. 445–452, Jun. 2014.

[26] L. Zhang, Z. Wang, X. Hu, F. Sun, and D. G. Dorrell, "A comparative study of equivalent circuit models of ultracapacitors for electric vehicles," *J. Power Sources*, vol. 274, pp. 899–906, 2015.

[27] Z. Amjadi and S. S. Williamson, "Power-electronics-based solutions for plug-in hybrid electric vehicle energy storage and management systems," *IEEE Trans. Ind. Electron.*, vol. 57, no. 2, pp. 608–616, 2010.

[28] Y. Choi, N. Chang, and T. Kim, "DC-DC converter-aware power management for low-power embedded systems," *IEEE Trans. Comput.-Aid. Des.*, vol. 26, pp. 1367–1381, Aug. 2007.